

TCT

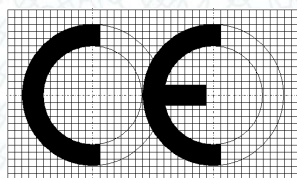
Certificate of Compliance

Certificate No. : TCT171219E025C
Applicant : Apias AS
Address : Austbøvegen 16, 5542 Karmsund, Norway
Manufacturer : Apias AS
Address : Austbøvegen 16, 5542 Karmsund, Norway
Product : Apias Smart Lightning Cable
Model No. : IPYSUSB01
Trade mark : N/A

The above products have been tested by us with listed standards and found in compliance with the council EMC 2014/30/EU. It is possible to use CE marking to demonstrate the compliance with this EMC.

Test standards:	Report(s) Number	Issued By	Issued Date
EN 55032:2012+AC:2013 EN 61000-3-2:2014 EN 61000-3-3:2013 EN 55024:2010+A1:2015	TCT171219E025	TCT	Dec. 25, 2017

The statement is based on a single evaluation of one sample of above mentioned products. It does not imply an assessment of the whole production and does not permit the use of the test lab logo.



Tomsin

Tomsin/Senior Engineer

Dec. 25, 2017



Shenzhen TCT Testing Technology Co.,Ltd.

Hotline: 400-6611-140 Tel: 86-755-27673339 Fax: 86-755-27673332 [Http://www.tct-lab.com](http://www.tct-lab.com)



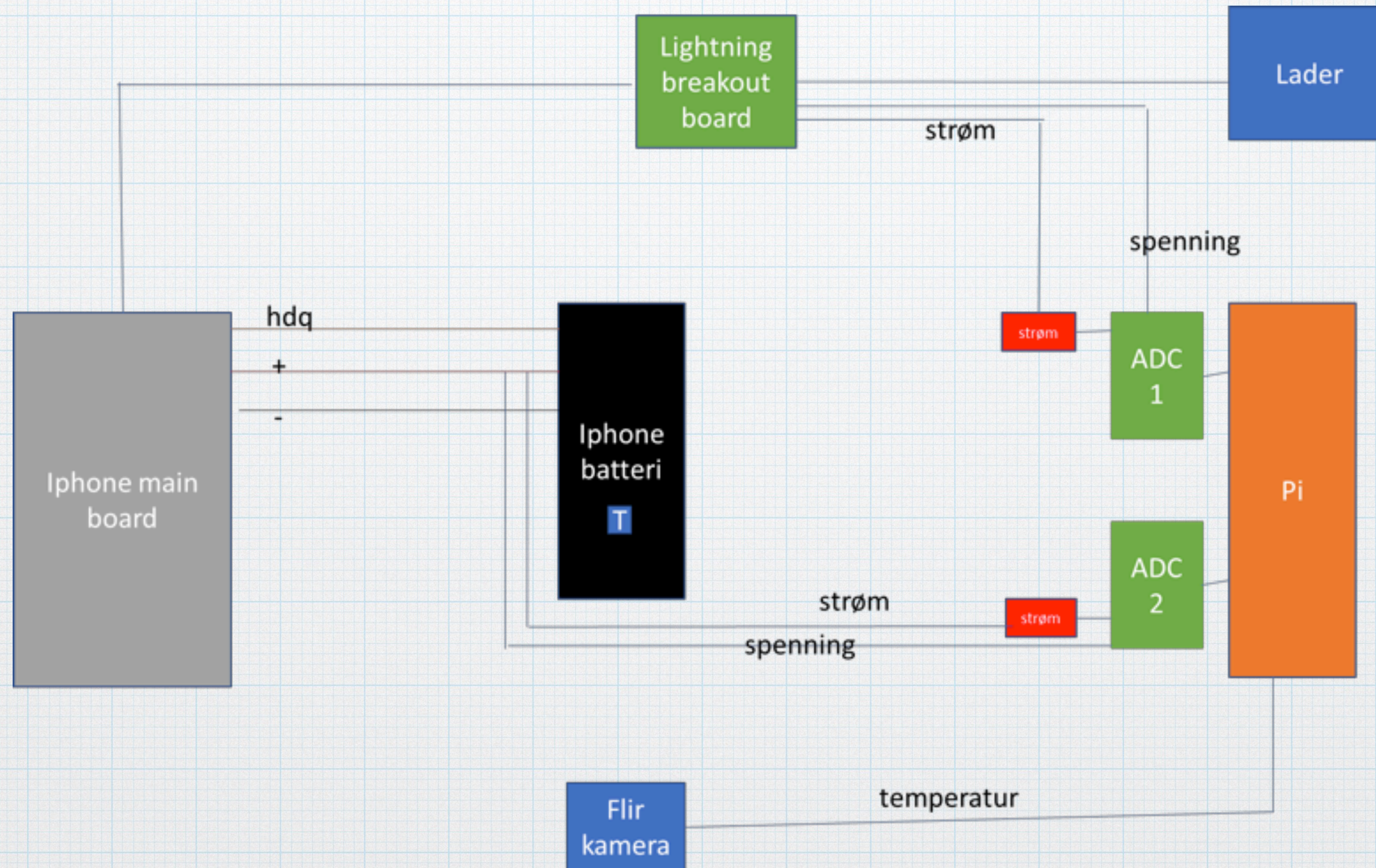
Test Report - apias

Polytec / Gas and material technology T-18035-R001

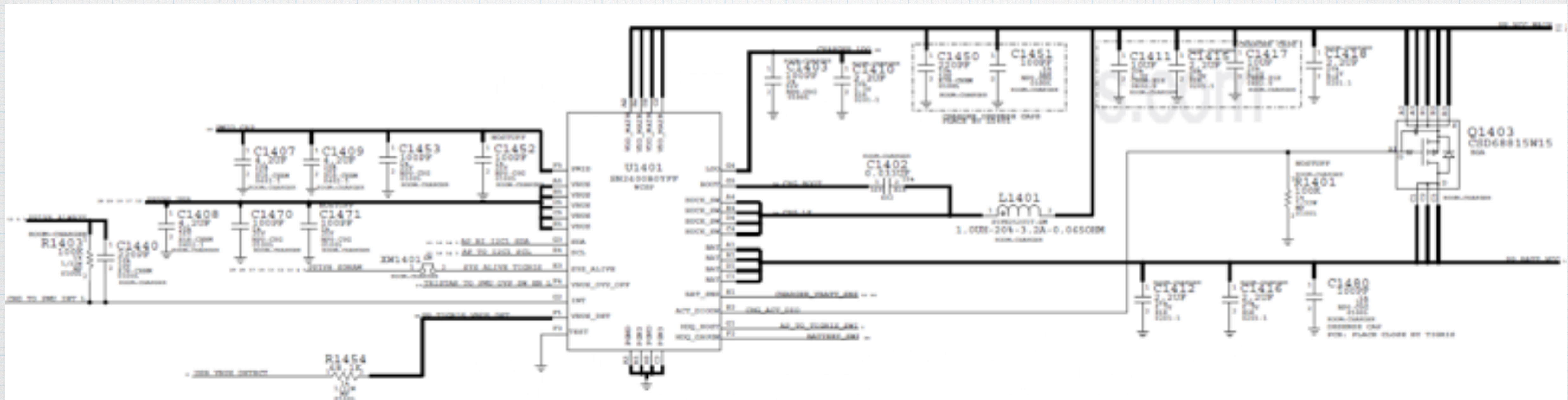
Summary

- * The test was conducted to examine how the phone's internal charging mechanism handles charging after the phone's battery is full.
- * Identical tests were performed with original charging cable from the supplier, and apias smart charging cable.
- * The same assumptions underlie all tests.

Test Rig

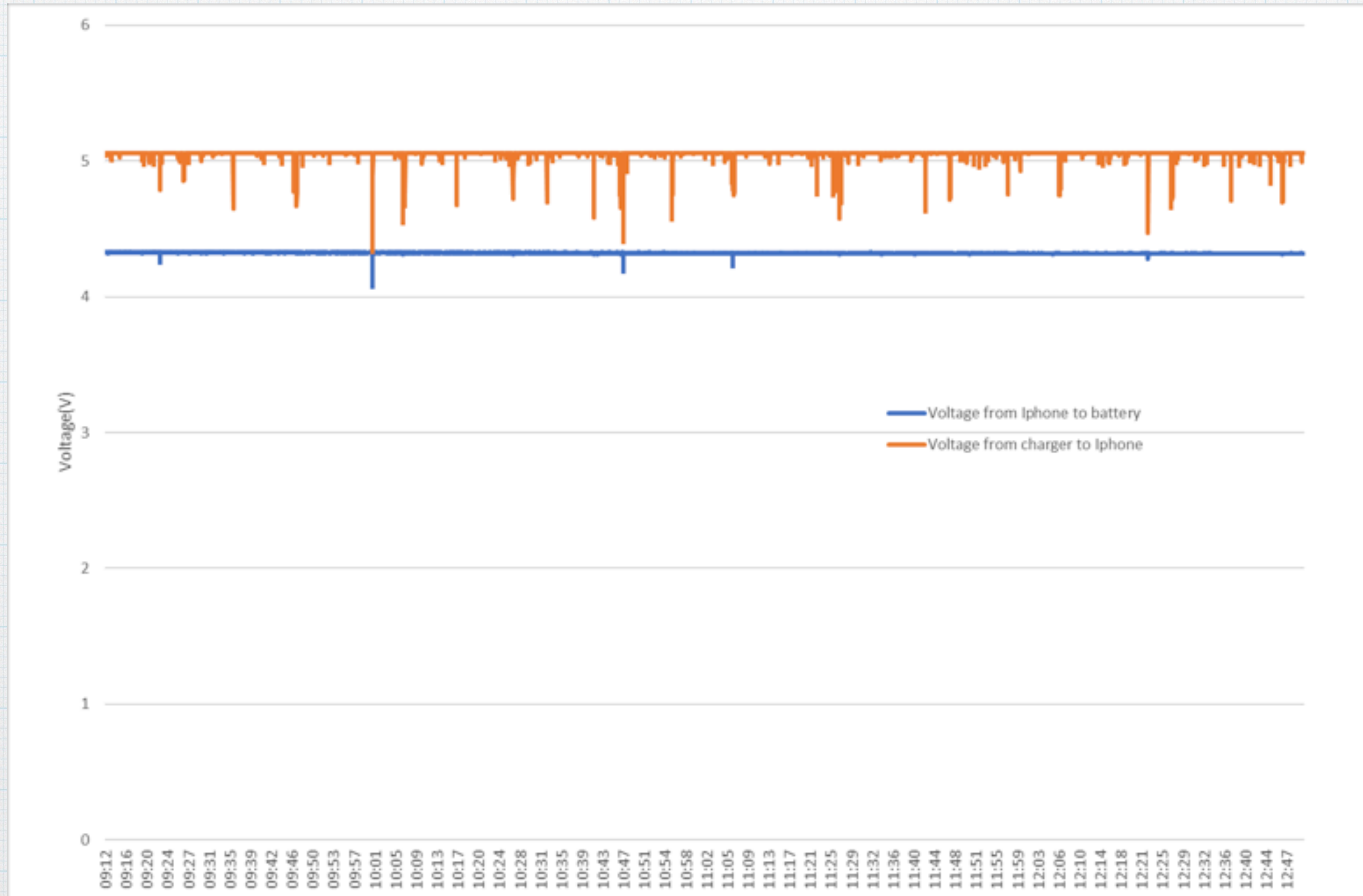


Charging Scheme - iPhone

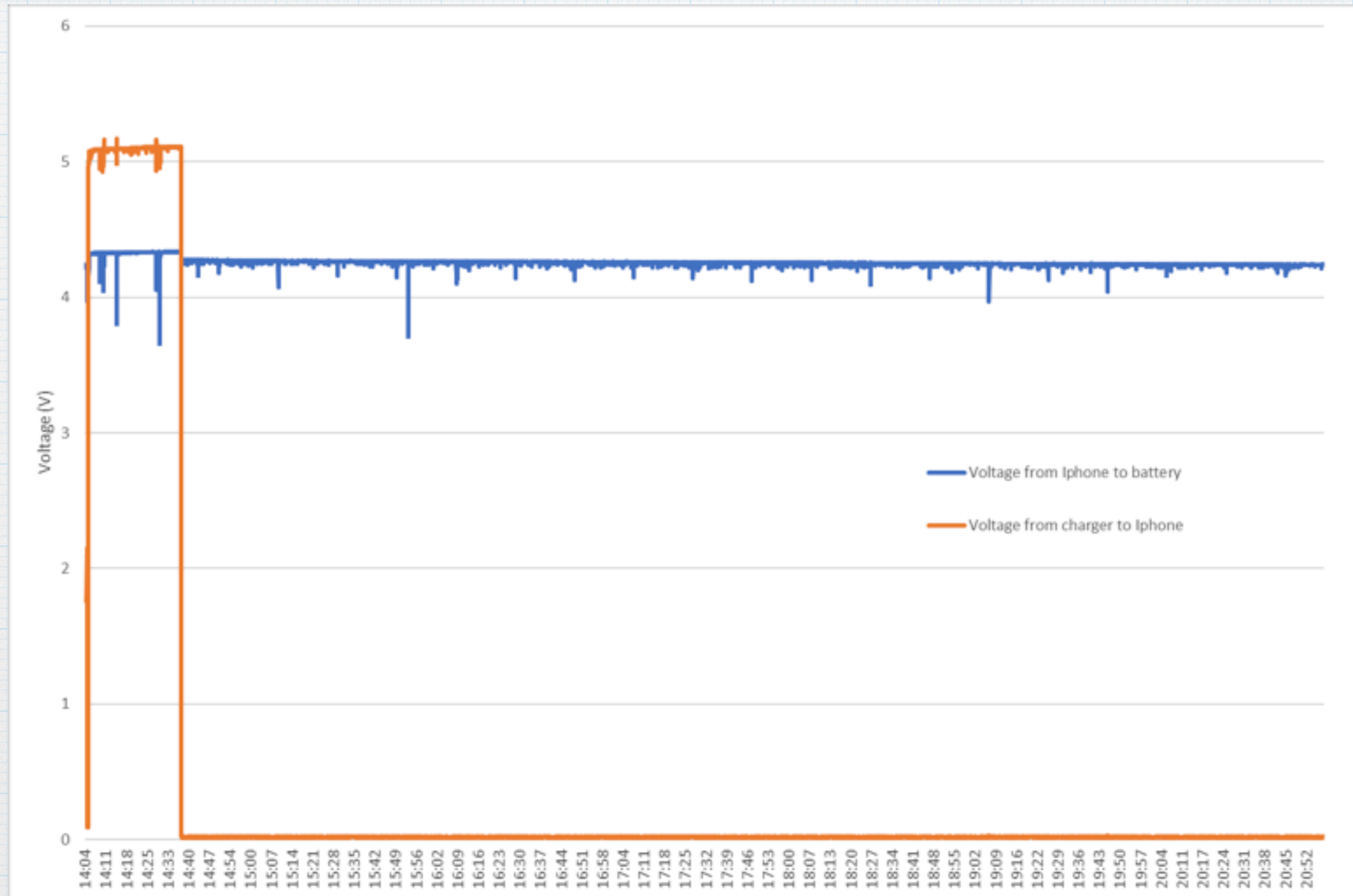


Bilde: Tigris IC connections

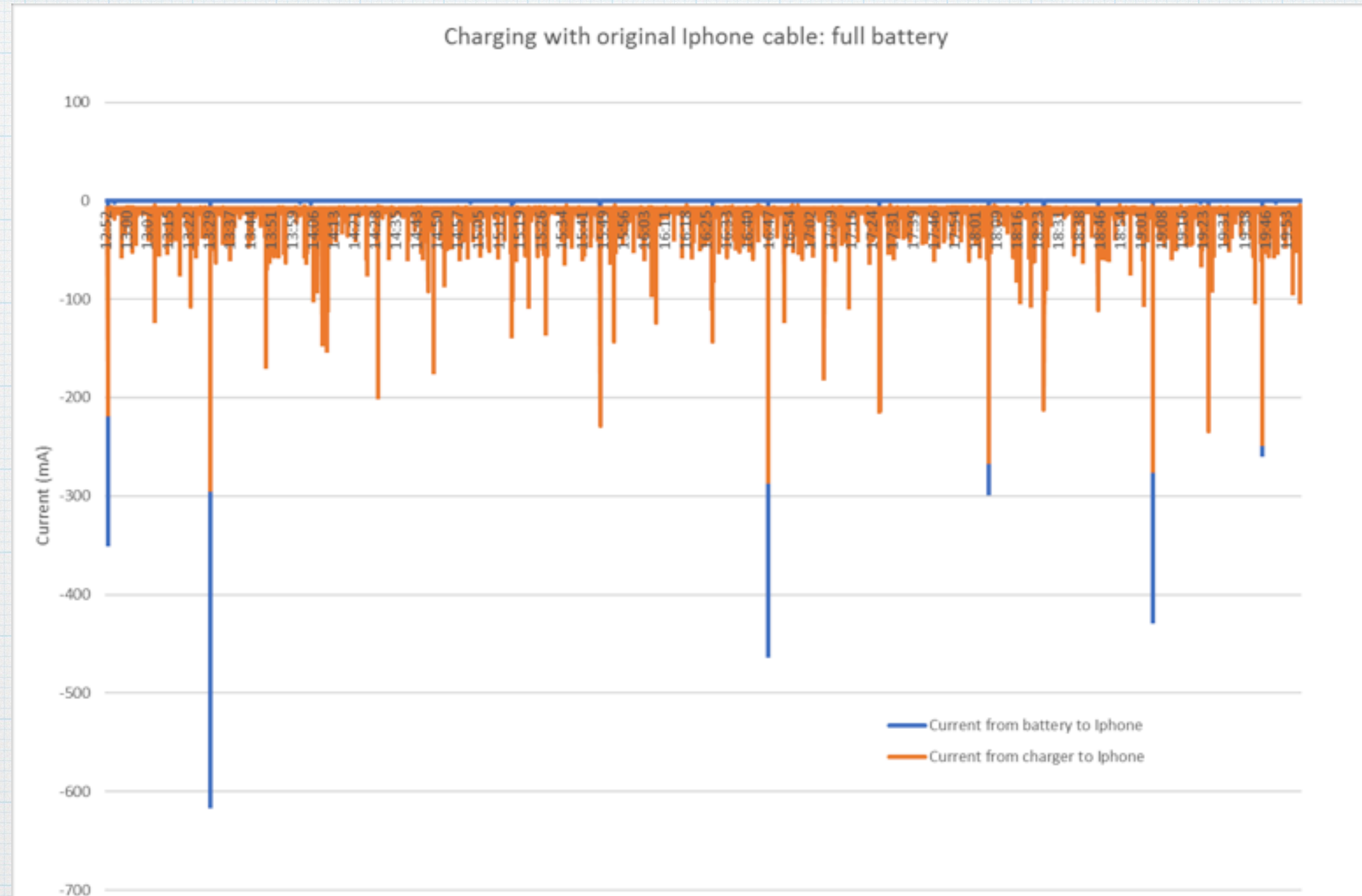
Volt: original cable



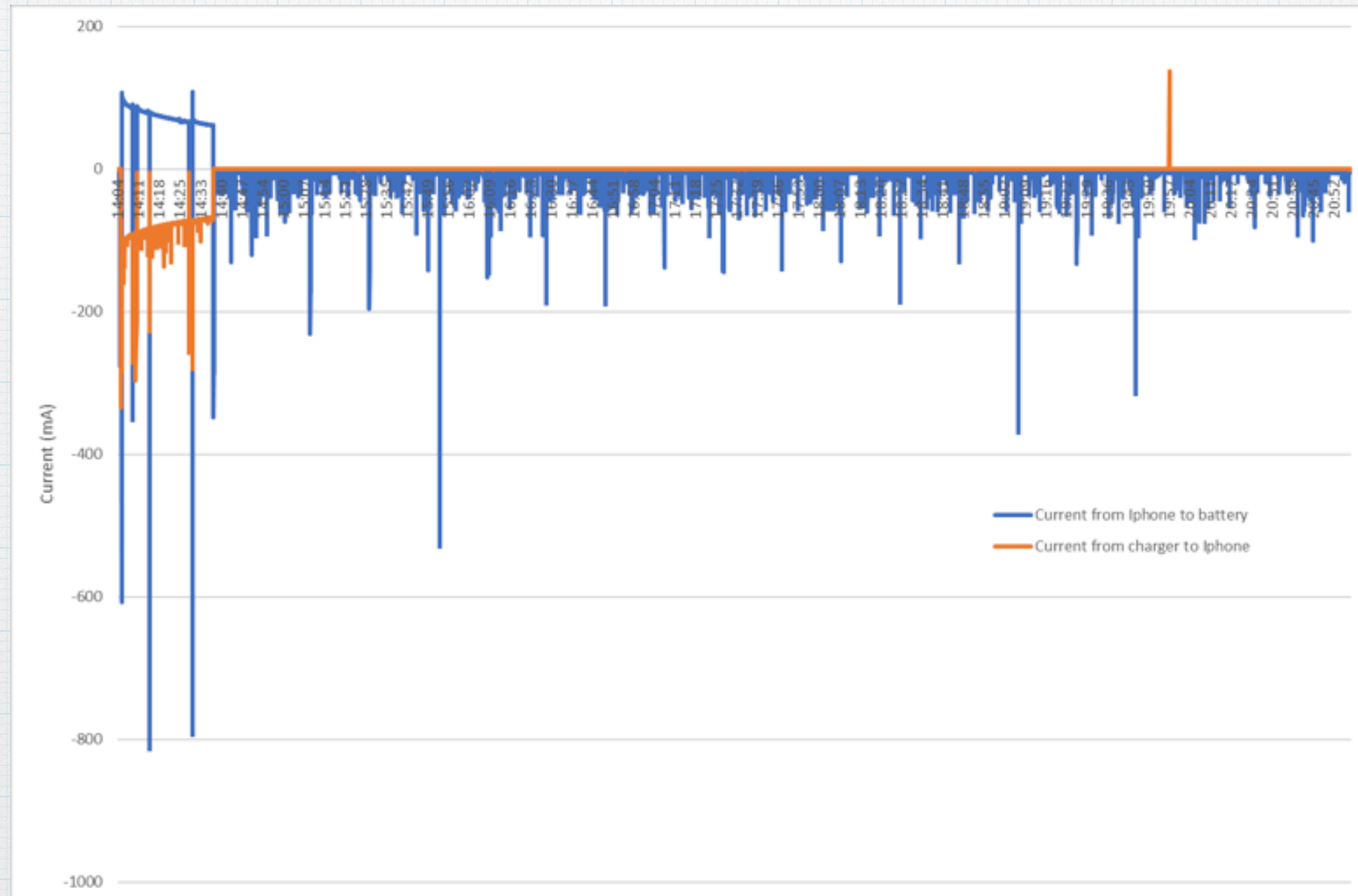
Volt: apias



Ampere: original cable



Ampere: apias



Conclusion

- * The test clearly verifies that using the original cable, is not disconnecting the battery once its full.
- * There is a significant difference in Amp using the two different cables.
- * The project establishes that the battery still maintains the closed circuit current after it is fully charged. Original wall adapter was used during both tests.



OPEN ACCESS

Electrode Stack Geometry Changes during Gas Evolution in Pouch-Cell-Type Lithium Ion Batteries

To cite this article: Toby Bond *et al* 2017 *J. Electrochem. Soc.* **164** A6158

View the [article online](#) for updates and enhancements.

EXTENDED ABSTRACT DEADLINE: DECEMBER 18, 2020

 **239th ECS Meeting**
with the 18th International Meeting on Chemical Sensors (IMCS) 

May 30-June 3, 2021 **SUBMIT NOW →**



FOCUS ISSUE OF SELECTED PAPERS FROM IMLB 2016 WITH INVITED PAPERS CELEBRATING 25 YEARS OF LITHIUM ION BATTERIES

Electrode Stack Geometry Changes during Gas Evolution in Pouch-Cell-Type Lithium Ion Batteries

Toby Bond,^z Jigang Zhou,^{*} and Jeffrey Cutler

Canadian Light Source Inc., Saskatoon, Saskatchewan S7N 2V3, Canada

Safety remains a significant concern for the lithium-ion battery industry, despite over twenty five years of development since their commercial introduction [R. Spotnitz and J. Franklin, *J. Power Sources*, **113**, 81, (2003)]. Many abusive conditions (such as overheating, overcharge, overdischarge, and electrical short) can give rise to gas evolution in lithium ion batteries, which causes increased pressure and/or expansion of the cell leading to changes in the electrode geometry that can lead to significantly different electrochemical performance and safety characteristics [Y. Qi, S. S. J. Harris, *J. Electrochem. Soc.*, **157**, A741 (2010)]. In order to characterize the cell-level changes that occur during gas evolution, a non-destructive technique is required that can image the internal components of the cell at high spatial resolution without perturbing the electrode assembly itself. This paper demonstrates the use of synchrotron-based computed tomography to characterize the changes in electrode geometry that occur during gas evolution in a commercial aluminum pouch cell.

© The Author(s) 2016. Published by ECS. This is an open access article distributed under the terms of the Creative Commons Attribution 4.0 License (CC BY, <http://creativecommons.org/licenses/by/4.0/>), which permits unrestricted reuse of the work in any medium, provided the original work is properly cited. [DOI: 10.1149/2.0241701jes] All rights reserved.



Manuscript submitted October 3, 2016; revised manuscript received November 8, 2016. Published November 22, 2016. This was Paper 995 presented at the Chicago, Illinois, Meeting of the IMLB, June 19–24, 2016. *This paper is part of the Focus Issue of Selected Papers from IMLB 2016 with Invited Papers Celebrating 25 Years of Lithium Ion Batteries.*

Lithium-ion batteries have been ubiquitous in consumer electronics since their commercial introduction over twenty five years ago. Today, lithium-ion batteries are now widely used in significantly more demanding environments such as electric vehicles, grid energy storage, and high-power industrial applications. These applications expose battery cells and packs to significantly more abusive conditions, including fast charge/discharge rates, high voltage, high temperature, and greater mechanical stress. Safety still remains a significant concern in the battery industry, and in order to ensure the safe operation of batteries under such stressful conditions, the effect of different abusive conditions must be well understood at the material, cell, and pack level.¹ There is a wide variety of cell form factors currently in commercial use, from cylindrical cells with rigid steel casings to pouch-cell based designs with flexible, polymer-coated aluminum casings. The volume, dimensions, and casing material of the cell can have a significant impact on how the cell responds to different types of abuse.² This study focuses on the physical behavior of the electrode assembly in a standard aluminum pouch-cell under abusive conditions.

Gas evolution in lithium-ion batteries is a frequently observed result of a variety of abuse conditions. Elevated temperature, overcharge, and overdischarge can all lead to evolution of various gases (such as oxygen, carbon dioxide, carbon monoxide, and methane) caused by the degradation of cell materials.^{3,4} Gas evolution also regularly occurs as part of the cell manufacturing process during the formation cycles (where the cell is initially charged and discharged under carefully controlled conditions).⁵ In cells with rigid casings, gas evolution will give rise to an increase in pressure, requiring some sort of venting mechanism to prevent a catastrophic explosion of the battery.⁴ In a sealed aluminum pouch cell, gas evolution will cause the flexible casing to swell from a regular rectangular prism into a pillow-shaped geometry. Although this swelling is routinely observed, the behavior of the electrode “jellyroll” assembly inside a swollen cell has not (to the authors’ knowledge) been studied. A jellyroll consists of double-coated electrode layers that are wrapped around each other in a concentric spiral with a polymer separator layer between them. This electrode geometry is ubiquitous in industry in both cylindrical and rectangular-prismatic form factors.⁶ In order to observe the change in geometry of the jellyroll, a non-invasive imaging technique is required. This study demonstrates the use of synchrotron-based computed tomography to

image the change in geometry of the electrode assembly in a commercial pouch cell before and after gas evolution due to overdischarge.

Experimental

Pouch cell and electrochemical procedure.—A commercially manufactured LiCoO₂/graphite pouch cell was acquired from a Chinese battery manufacturer. This pouch cell is a standard 200 mAh rectangular prismatic cell measuring 6 mm × 22 mm × 34 mm. The rated discharge and charge voltage limits of the cell are 2.75 V to 4.2 V, respectively, with a nominal operating voltage limit of 3.7 V. The electrolyte consists of a LiPF₆ salt in a standard carbonate-based solvent.

A Neware BTS 3000 charger was used to charge and discharge the cell. The cell was first imaged at 50% state-of-charge with an open-circuit voltage of 3.7 V. After the imaging was complete, the cell was discharged to −500 mV (at a rate of 2C) and held at that voltage to ensure the production of gas in the cell. Swelling of the cell was observed in the last minute of discharge as the voltage approached zero. Previous work indicates that the gases produced by overdischarging a LiCoO₂/graphite cell include CO₂, CO, and CH₄.⁷

Synchrotron-based computed tomography.—Computed tomography (CT) was used to image the electrode assembly in 3D before and after overdischarge in a non-invasive manner. CT is a well-known X-ray imaging technique that involves collecting a series of 2D radiographic projections of a sample at different angles, then reconstructing these projections into a 3D image, where every voxel in the dataset represents the X-ray absorption value of a given material.⁸ In order to collect high-resolution data in a reasonable timescale, synchrotron-based CT was used, which allows for the acquisition of CT images with better contrast and much faster collection times than can be achieved with laboratory-based CT.⁹ Synchrotron-based CT has seen increasing use in the battery community as a tool for investigating failure mechanisms and imaging physical changes within the cell.¹⁰

CT scans were carried out at the Canadian Light Source on the Biomedical Imaging and Therapy Bending Magnet (BMIT-BM) beamline. The beamline was run in “white beam” mode with a set of high-pass filters inserted upstream of the pouch cell so that the incident X-rays were within an energy range of 30–40 keV. The X-ray images were acquired using an Orca Flash high-speed camera coupled with an X-ray scintillator. The pouch cell was placed at

^{*}Electrochemical Society Member.

^zE-mail: toby.bond@lightsources.ca

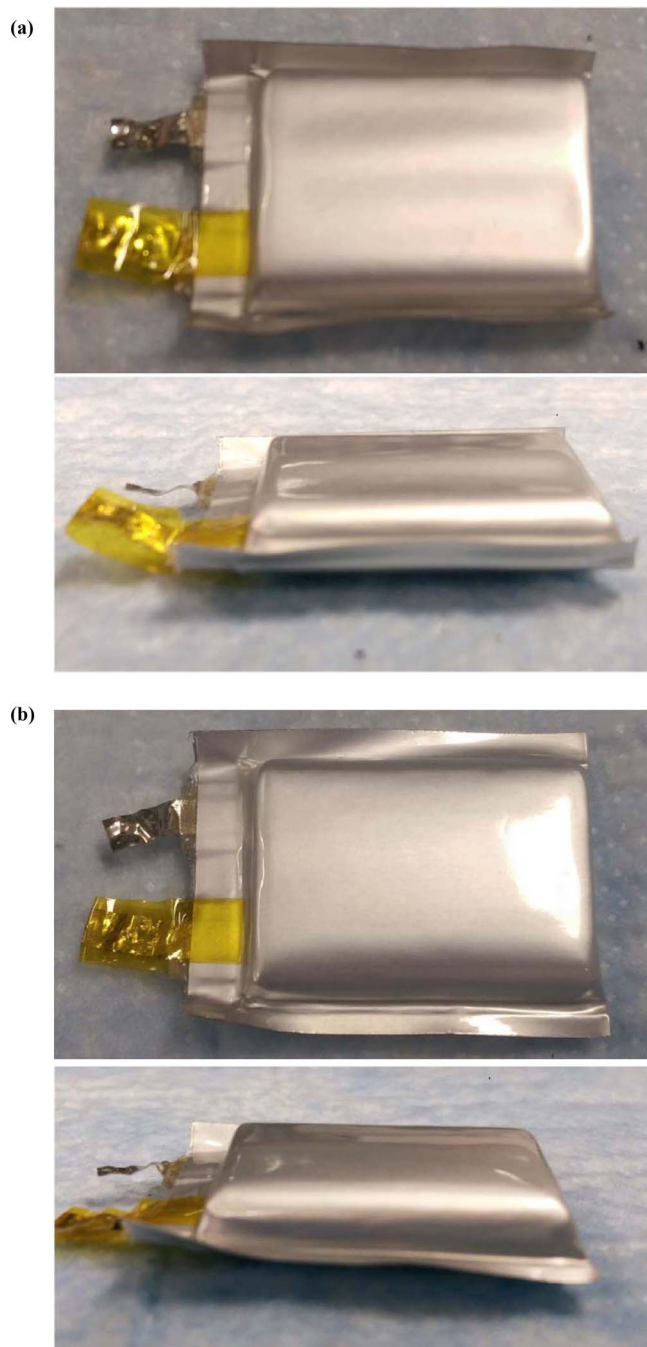


Figure 1. Photographs of the pouch cell imaged using synchrotron CT (a) before and (b) after overdischarge to -500 mV.

a sample-detector distance of 20 cm to maximize spatial resolution. The effective pixel dimensions of the images collected under these conditions were measured to be 13.024×13.024 microns.

The height of the X-ray beam under these conditions was 2.0 mm, so in order to image the entire cell, a stack of overlapping slices was collected, then stitched together during data processing. The total data acquisition time for each full CT scan of the cell was less than 30 minutes. This is over an order of magnitude faster than a comparable lab-based micro CT system, making synchrotron-based CT a time-efficient means of imaging the micron-level features of a commercial electrode assembly. Background and noise correction were carried out using ImageJ and reconstruction was carried out using the Nrecon software package.¹¹ Visualization and quantitative

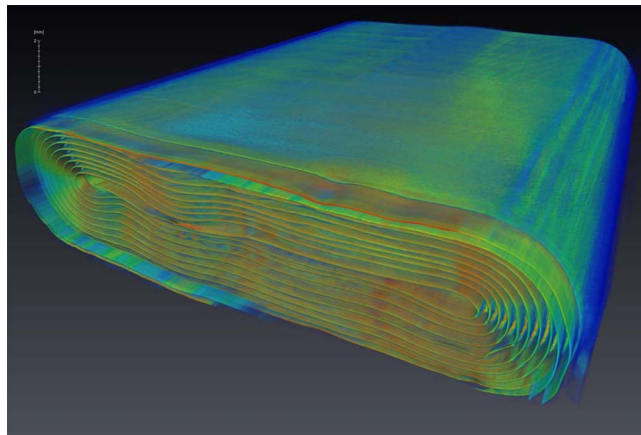


Figure 2. Full three-dimensional rendering of jellyroll assembly inside the pouch cell. The heat map denotes the X-ray absorption value of the material (which is represented in greyscale for the remaining figures).

analysis of the data was carried out using the Avizo 9.0 software package.

Results and Discussion

Photographs of the pouch cell imaged in this paper are shown in Figure 1, where the same cell is pictured (a) before and (b) after it was overdischarged to -500 mV. The swelling of the aluminum/Mylar cell casing is clearly visible in these pictures, indicating that gas has been produced in the cell. As previously mentioned, the gas produced is likely a combination of CO_2 , CO , and methane.

Figure 2 shows the full 3D rendering of the cell created from the CT scan before overdischarge. This false-color rendering shows the jellyroll electrode assembly with the copper current collector “overhang” region clearly visible. The heaviest elements in the pouch cell are cobalt (from LiCoO_2) and copper (from the graphite current collector foil), both of which are significantly heavier than aluminum, carbon, fluorine, oxygen, and lithium (which comprise all remaining materials in the cell). An incident X-ray beam of high energy (short wavelength) must be used in order to penetrate the pouch cell at all angles, which also reduces the contrast in X-ray absorption between various materials. In this image, the beam has a broad energy distribution in the region of 30–40 keV, which is sufficient to penetrate the positive electrode material and copper foil from the negative electrode layer. However, this yields a very low X-ray absorbance (and corresponding image gray value) for the graphite electrode layer itself, as well as the aluminum foil current collector (from the positive electrode layer), polymer separator material, and aluminum cell casing. In most of the CT scan, these lighter materials are indistinguishable from each other and from air. It is important to note that all images in this paper are thus dominated by the LiCoO_2 electrode layer and the copper foil from the graphite layer. The less-absorbing materials often appear simply as dark space between these highly-absorbing layers.

Figures 3a and 3b show cross sections taken from the longitudinal center of the cell before and after overdischarge (respectively) to -100 mV. To align the two CT scans for comparison, the 3D models of the cells were first manually aligned in the analysis software so that they were in a similar orientation (to provide a starting point for the alignment algorithm). The alignment algorithm then performs a least-squares regression which minimizes the magnitude of the difference between the two datasets by systematically rotating and translating one model relative to the other. This process effectively uses the unchanged parts of the cell as a reference, since aligning those sections provides the smallest total difference value. Through this process, alignment of the turns in the jellyroll yielded the best result from the regression, indicating that there was very little geometric change in those areas.

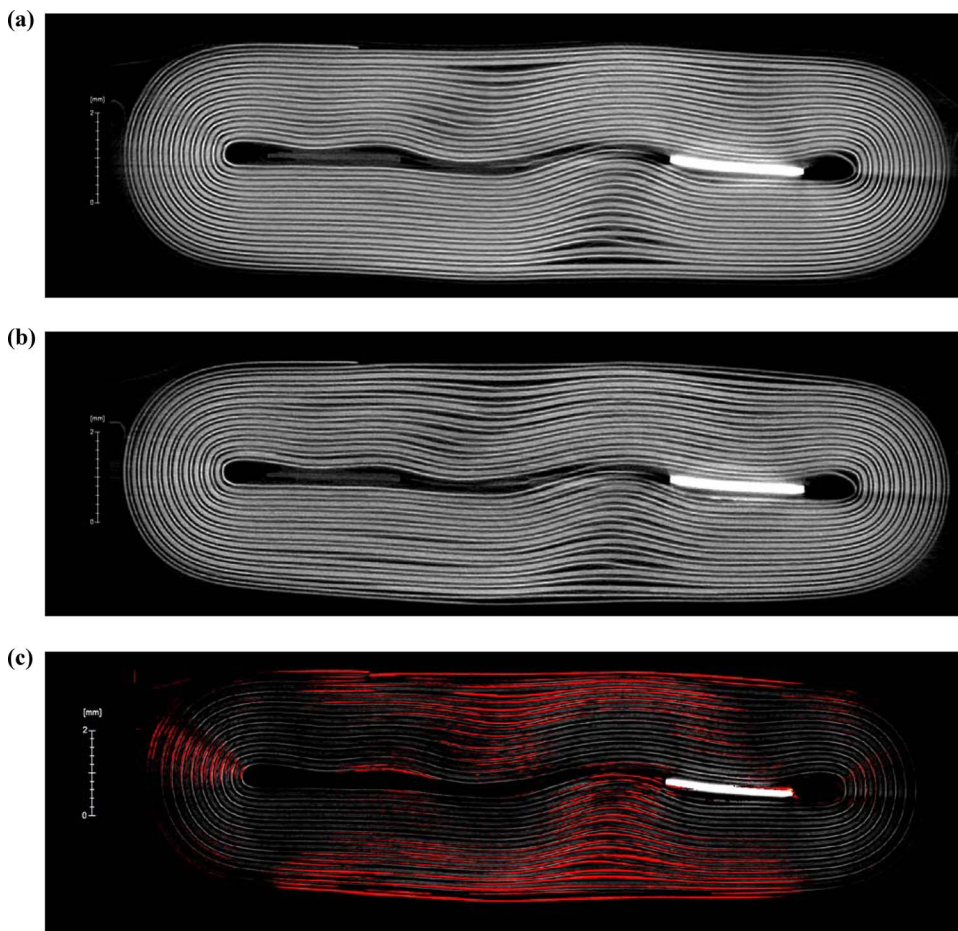


Figure 3. Two-dimensional cross-sections taken from the longitudinal center of the pouch cell for (a) the before-overdischarge CT scan and (b) the after-overdischarge scan. The image shown in (c) is a difference map of the two scans, where the red color indicates the difference in gray value between the cross sections in (a) and (b).

A preliminary comparison of these two images shows that there is expansion along the vertical axis of the jellyroll stack and increased gaps between electrode layers on the flat section of the jellyroll. To highlight exactly where these differences are, a difference map was created where the gray value of every pixel in the after-discharge CT was subtracted from each corresponding pixel in the aligned before-discharge CT scan. This difference map is shown in Figure 3c, where the red color indicates the magnitude of the difference between gray value of the two scans. A greyscale image (with reduced brightness) of the pre-discharge scan is also included in the background of this image for reference. This image shows in finer detail exactly where and to what extent the displacement of electrode layers occurs. A notable feature of this image is that there is very little displacement in the circular turns of the electrode (at the left and right edges of the image) and most of the displacement occurs in the flat portion of the jellyroll, along the minor axis (i.e. the axis along the shortest dimension) of the pouch cell. The other major notable feature of the difference map is that the greatest displacement occurs in areas where there is already a deformity in the jellyroll structure (before overdischarging of the cell). These deformed areas are highlighted in red on the difference map. This result suggests that the stack pressure along the minor axis is reduced in these areas where there is a wrinkle or other deviation from the ideal jellyroll geometry.

Figure 4a shows a plot of gray value (i.e. X-ray absorption) as a function of distance from the center of the jellyroll for the before- and after-overdischarge CT scans. The strip of pixels used to generate this plot is highlighted in orange in Figure 4b. The narrower, single peaks in this plot correspond to the copper foil from the negative current

collector, while the broader, merged double peaks correspond to the double coated layer of LiCoO_2 (with the dip between the doublets indicating the aluminum foil current collector onto which the LiCoO_2 is deposited). This plot shows a typical example of how the electrode layers expand from the center as a result of the gas evolution. The peaks in the plot are displaced to an increasingly greater extent from their original position as the distance from the center of the jellyroll increases. This profile is consistent along the rest of the cell along the flat portion of the jellyroll. The average axial expansion of the entire jellyroll along the minor axis was measured to be 6.27%, while the axial expansion along the long axis connecting the two circular turns of the jellyroll was measured to be only 0.23%. There was no longitudinal expansion measured at this resolution.

Figures 5a and 5b show close-up longitudinal sections of the graphite overhang region (from one edge of the cell) taken from the CT scans before and after overdischarge, respectively. These longitudinal sections were both taken at the center of the flat portion of the jellyroll. A difference map of these two images is shown in Figure 5c. The same uniform expansion of the electrode layers along the minor axis of the cell is clearly visible in the difference map, where both the LiCoO_2 and graphite overhang show significant expansion in a pattern similar to that shown in Figure 4. Figures 6a and 6b show difference maps for both overhang regions in the plane perpendicular to the minor axis of the pouch cell. These longitudinal sections are in the center of the circular turns in the pouch cell, which did not exhibit significant expansion as seen in the cross-sections images of Figure 3. The difference map in this case does exhibit some minor expansion (with the more expansion toward the outside of the jellyroll), but it

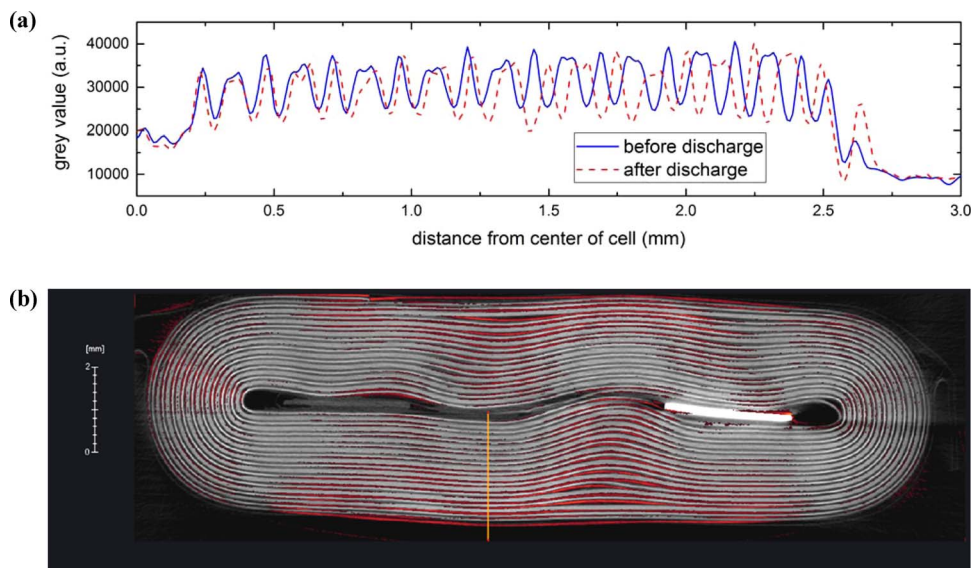


Figure 4. (a) a plot of gray value (X-ray absorption) as a function of distance from the center of the jellyroll cross-section. The strip of pixels used to generate this plot is highlighted in orange in figure (b).

is to a significantly lesser extent than the expansion along the minor axis observed in Figure 4.

Conclusions and Future Work

This work demonstrates the use of synchrotron-based CT as an effective and time-efficient method for imaging the internal change

in electrode geometry due to cell abuse. The results of these scans indicate that most of the change in the electrode geometry occurs along the minor axis of the cell in the flat portion of the jellyroll. The greatest expansion of electrode layers occurred in areas where the jellyroll was already deformed prior to abuse, indicating that the stack pressure in these deformed regions is lower than in the rest of the assembly. The fact that jellyroll expansion due to gas-evolution is

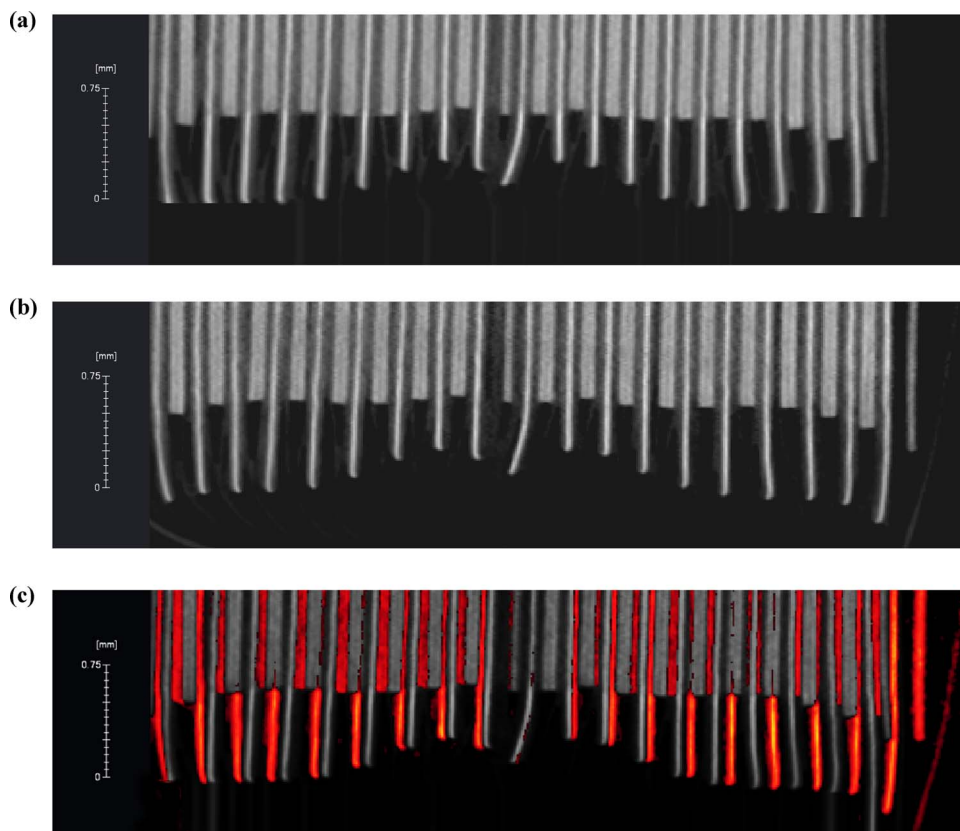


Figure 5. Two-dimensional longitudinal-sections taken from an edge of the pouch cell (parallel to the narrowest cell dimension). These sections were taken from (a) the before-overdischarge CT scan and (b) the after-overdischarge scan. The image shown in (c) is a difference map of the two scans, where the red color indicates the difference in gray value between the cross sections in (a) and (b).

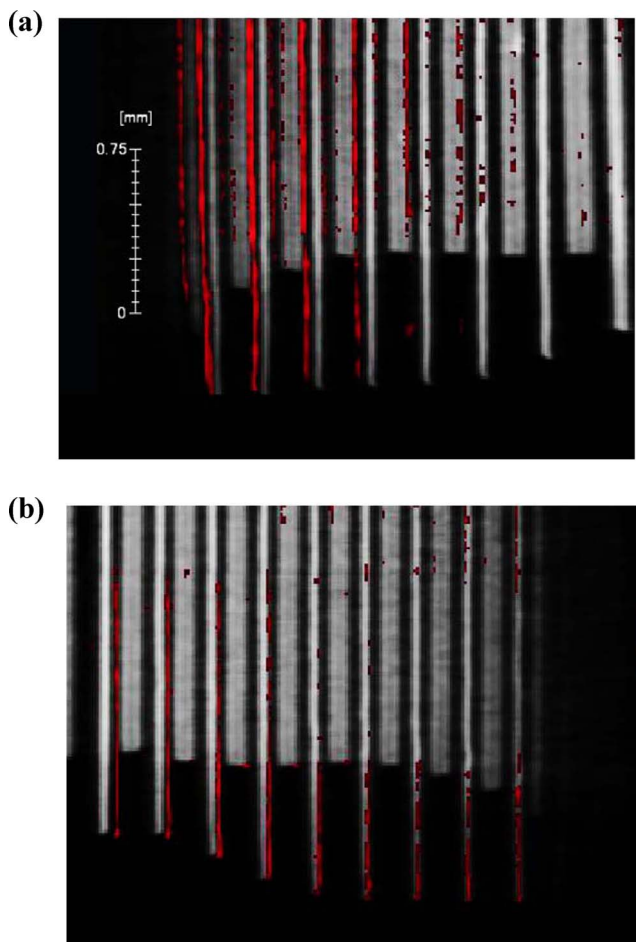


Figure 6. Two-dimensional longitudinal-sections taken from an edge of the pouch cell (parallel to the widest cell dimension). Image (a) shows the layers of electrode overhang on one of the two circular turns of the jellyroll while image (b) shows the same area for the other circular turn.

non-uniform in this manner has not been previously reported to the authors' knowledge. Since the observed changes in cell geometry would likely impact the distribution of residual strain in the assembly, it's likely that the electrochemical performance and safety characteristics of the cell would also be impacted. Although the cell studied here was

rendered inoperative by overdischarging to a negative cell voltage, gas generation has been known to occur during normal operation of commercial cells. Gas evolution can result from a variety of abuse conditions and cell failure mechanisms, and a better understanding of how the cell responds to gas evolution is important to predict cell behavior under abusive conditions and improve cell design to better accommodate this behavior.

Only one type of cell (i.e. a rectangular prismatic pouch cell) was investigated in the present study, but there are many different form factors in use, including cylindrical geometries, rigid containers, and large-format electric vehicle cells. The effect of gas evolution on the electrode assembly is likely to be very different for each these form factors and an important avenue of investigation will be the application of high-resolution synchrotron CT to non-destructively image the subtle changes in electrode geometry under a variety of commercially relevant conditions.

Acknowledgments

Research described in this paper was performed using Biomedical Imaging and Therapy Bending Magnet (BMIT-BM) beamline at the Canadian Light Source. The authors thank George Belev, Ning Zhu, and Adam Webb for their assistance. This beamline is supported by the Canadian Foundation for Innovation, the Natural Sciences and Engineering Research Council of Canada, the National Research Council Canada, the Canadian Institutes of Health Research, the Government of Saskatchewan, Western Economic Diversification Canada, and the University of Saskatchewan.

References

1. R. Spotnitz and J. Franklin, *J. Power Sources*, **113**, 81, (2003).
2. Y. Qi and S. S. J. Harris, *J. Electrochem. Soc.*, **157**, A741 (2010).
3. K. H. Lee, E. H. Song, J. Y. Lee, B. H. Jung, and H. S. Lim, *J. Power Sources*, **132**, 201 (2004).
4. W. H. Kong, H. Li, X. J. Huang, and L. Q. Chen, *J. Power Sources*, **142**, 285 (2005).
5. B. Zhang, M. Metzger, S. Solchenbach, M. Payne, S. Meini, H. A. Gasteiger, A. Garsuch, and B. L. Lucht, *J. Phys. Chem.*, **119**, 11337 (2015).
6. T. Wierzbicki and E. Sahraei, *J. Power Sources*, **241**, 467 (2013).
7. N. S. Spinner, C. R. Field, M. H. Hammond, B. A. Williams, K. M. Myers, A. L. Lubrano, S. L. Rose-Pehrsson, and S. G. Tuttle, *J. Power Sources*, **297**, 713 (2015).
8. P. Tafforeau, R. Boistel, E. Boller, A. Bravin, M. Brunet, Y. Chaimanee, P. Cloetens, M. Feist, J. Hoszowska, J. J. Jaeger, R. F. Kay, V. Lazzari, L. Marivaux, A. Nel, C. Nemoz, X. Thibault, P. Vignaud, and S. Zabler, *Applied Physics A-Materials Science and Processing*, **83**, 195 (2006).
9. A. Momose, *Japanese Journal of Applied Physics*, **44**, 6355 (2005).
10. D. Devaux, K. J. Harry, D. Y. Parkinson, R. Yuan, D. T. Hallinan, A. MacDowell, and N. P. Balsara, *J. Electrochem. Soc.*, **162**, A1301 (2015).
11. C. A. Schneider, W. S. Rasband, and K. W. Eliceiri, *Nature Methods*, **9**, 671 (2012).